Journal of Hazardous Materials 186 (2011) 1174–1182

Contents lists available at ScienceDirect

Journal of Hazardous Materials

journal homepage: www.elsevier.com/locate/jhazmat

Characterization and application of Ti-containing mesoporous silica for dye removal with synergistic effect of coupled adsorption and photocatalytic oxidation

Chih-Hung Huang[a], Kai-Ping Chang[a], Hong-De Ou[a], Yu-Chun Chiang[b], E.-E. Chang[c], Chu-Fang Wang[a,d,*]

[a] Graduate Institute of Biomedical Engineering and Environmental Sciences, National Tsing Hua University, Hsinchu 30013, Taiwan, ROC
[b] Department of Mechanical Engineering, Yuan Ze University, Taoyuan 32003, Taiwan, ROC
[c] Department of Biochemistry, Taipei Medical University, Taipei, Taiwan, ROC
[d] Graduate Institute of Nuclear Engineering and Science, National Tsing Hua University, Hsinchu 30013, Taiwan, ROC

ARTICLE INFO

Article history:
Received 19 July 2010
Received in revised form
29 November 2010
Accepted 29 November 2010
Available online 4 December 2010

Keywords:
Adsorption
Photocatalytic oxidation
Dye
Mesoporous
TiSBA-15

ABSTRACT

Highly ordered mesoporous silica, Santa Barbara Amorphous-15 (SBA-15), and titanium-substituted mesoporous silica (TiSBA-15) materials were successfully synthesized, characterized, and evaluated. The textual and structural properties of the prepared materials with various titanium contents were characterized by inductively coupled plasma-mass spectrometer (ICP-MS), powder X-ray diffraction (XRD) patterns, nitrogen physisorption isotherms, scanning electron microscopy (SEM), and transmission electron microscopy (TEM). A limited content of titanium could be effectively substituted into the framework of SBA-15 without provoking structure change. The adsorptive performance was examined by methylene blue (MB) adsorbed on prepared materials. The isotherm models were analyzed to describe the adsorption behavior of prepared materials. The adsorption isotherms were well-fitted with Langmuir and Freundlich models in the simulation of the adsorption behavior of dyes. The SBA-15 and TiSBA-15 materials were found to be effective adsorbents for MB from aqueous solutions. The photodegradation of MB and total organic carbon (TOC) analysis on solid composites were used to evaluate the catalytical performance of Ti-containing mesoporous silica. The synergistic effect of adsorptive and photocatalytical ability of prepared TiSBA-15 was identified. The regeneration and cyclic performance were also proved. These results revealed that TiSBA-15 could be one effective alternative material for dye removal.

1. Introduction

The effluents of wastewater from textile industries are highly colored and contain many toxic and refractory organic compounds which can cause severe environmental damages. It is noteworthy that even a small amount of dyes discharged into water can affect the aquatic ecosystem. Dyes are also known to be carcinogenic and mutagenic for aquatic organisms [1]. Therefore, the dye removal from colored effluents has attracted increasing attention. Various physical, chemical and biological dye removal techniques from aqueous solutions have developed [2] and further classified as follows:

(A) Physico-chemical methods: adsorption on activated carbon, zeolite [3–7].
(B) Filtration techniques: micro/ultra/nano-filtration, reverse osmosis, ion exchange process [8–12].
(C) Sedimentation/precipitation treatment with coagulation/flocculation, electrochemical methodology [13–15].
(D) Advanced oxidation processes (AOPs): Fenton's reagent, photo-Fenton process, ultra-violet photolysis, sonochemical degradation, ozonation [16–20].
(E) Biological treatment: biodegradation, enzymatic decomposition [21,22].

Generally, physical techniques only transfer organic compounds from water to another phase thus create secondary pollution. A further treatment of wastes and regeneration of the adsorbent is demanded which will cost more to the process. Although chemical techniques are vigorous ways for dye removal, they are often expensive and the accumulation of concentrated sludge after decolorization results in a disposal problem. Besides, a secondary pollution problem may arise due to the excessive chemical use. Biological

* Corresponding author at: Graduate Institute of Biomedical Engineering and Environmental Sciences, National Tsing Hua University, Hsinchu 30013, Taiwan, ROC. Tel.: +886 3 5715131.
E-mail address: cfwang@mx.nthu.edu.tw (C.-F. Wang).

0304-3894/$ – see front matter © 2010 Elsevier B.V. All rights reserved.
doi:10.1016/j.jhazmat.2010.11.125

method is often the most common and economical technique and offers significant advantages such as relatively inexpensive, low operation cost and the completely mineralized final products. However, the demand of a large land area and less flexibility in design and operation are the confinements on biological methodology.

Recent studies have devoted on the area of photocatalytic degradation and heterogeneous photocatalysis in the dye removal. Heterogeneous photocatalysis is considered an attractive and highly efficient method to degrade the toxic and non-biodegradable organic pollutants in environments. The process is based on the excitation of semiconductor material under UV radiation. The following redox reaction is initiated and the oxidation of the pollutants is performed on the excited surface. The advantages of this photocatalytical methodology include the potential of solar light utilization, no sludge production, reduction of COD, and the capability to completely mineralize the target pollutants. TiO_2 is a well-known photocatalyst with a bandgap of 3.2 eV of anatase form, which makes it suitable for UV exposure. TiO_2 is photocatalytically stable, chemically and biologically inert, commercially available, and environmentally friendly [23]. It has been known that the degradation rate of TiO_2 in heterogeneous photocatalysis largely depends on the adsorption capacity which is associated with the specific surface area [24]. However, there are some basic restrictions using the traditional TiO_2 nanoparticles, such as the immobilization and dispersion problem of nanoparticles, recycling problem, and the low transmission of radiation source. These problems are promoted by supporting nanosized TiO_2 particles onto the mesoporous materials, or incorporating them into the mesostructure.

The discovery of mesoporous silica such as SBA-15 (Santa Barbara Amorphous-15) has broadened the application of porous materials in adsorption and catalysis. The hexagonally arranged and highly ordered SBA-15 possess many advantages such as high surface area, large pore volume, tunable pore size, thick pore wall, good stability, and good performance as effective adsorbents [25]. The specific porous structure and excellent textual properties allow easier diffusion of reactive molecules before and after reactions, which make SBA-15 an ideal catalytic support.

Since one perfect method/system is practically difficult, combination of methodologies/system is preferable. The conjunction of adsorption and photocatalysis is considered as an effective and potential method to achieve a rapid removal of dyes from wastewater. Dye molecules are supposed to be adsorbed in situ environment and then photodegraded in factories. Dong et al. [26] reported a synchronous role of coupled adsorption and photocatalytic oxidation on ordered 2-D hexagonal mesoporous TiO_2–SiO_2 nanocomposites. The synchronous role results in excellent photocatalytic degradation activities which is much higher than that of Degussa commercial P25 photocatalyst. Organic pollutants are supposed to be adsorbed or concentrated in situ and then photo-degraded in vitro under factory process, while these mesoporous photocatalysts are regenerated and recycled. To the best of our knowledge, the synergistic effect, regeneration capability, and cyclic usability of TiSBA-15 materials are seldom completely investigated. For this reason, mesoporous SBA-15 and TiSBA-15 materials were synthesized and characterized in this study. The adsorption behavior was analyzed and compared by isotherm models, while the photodegradation performance of dyes on TiSBA-15 was also examined in order to identify the synergistic effect with adsorptive and photocatalytical ability.

2. Experimental

In this study, all chemicals, the preparation method, and the characterization techniques are described below. SBA-15 and TiSBA-15 samples were synthesized using a nonionic-surfactant-templating approach following the procedure reported by Vinu et al. [27]. Analytical techniques were used in order to characterize all prepared samples and clearly establish the physical and chemical properties.

2.1. Materials

Poly(ethylene glycol)-*block*-poly(propylene glycol)-*block*-poly(ethylene glycol) (P123, $EO_{20}PO_{70}EO_{20}$, M_w = 5800, BASF) and hydrochloric acid (HCl, 37.8%, J.T. Baker) were used in the synthesis of SBA-15 and TiSBA-15 materials as the structure-directing agent and catalyst, respectively. As precursors of Si and Ti, tetraethyl orthosilicate (TEOS, 99%, Merck) and titanium tetraisopropoxide (TTIP, $Ti(OC_3H_7)_4$, 99%, Acros.) were used. Methylene blue (MB, Merck) as the relatively bulky molecule represented a basic-dye system with well-know properties (basic-dye 9 (C.I. 52015); solid; λ_{max} = 663 nm; ε = 170.1 $dm^3\ g^{-1}\ cm^{-1}$; M = 320) and was selected as a model dye system.

2.2. Preparation method

SBA-15 and TiSBA-15 samples with different *n*Si/*n*Ti ratios 7, 5, 3 and 1 were synthesized with the following molar gel composition: 0.001 P123/0.237 HCl/8.3 H_2O/0.043 TEOS/(0, 0.006, 0.009, 0.014 and 0.043) TTIP. The solid products were denoted as TiSBA-15[X], where X stands for A, B, C and D which represents the *n*Si/*n*Ti = 7, 5, 3 and 1 in the initial gels, respectively. In a typical synthesis, 8.0 g of pluronic P123 was dissolved in 274.1 ml of distilled water and stirred at 35 °C for 2 h. Thereafter, 39.2 ml of HCl was then added to the clear solution and stirred for another 1 h. 19.3 ml of TEOS and the required amount of desired Ti source were added dropwise to the acid solution under vigorous stirring at 35 °C for 20 h. The resultant mixture was transferred into a polypropylene bottle and aged at 80 °C for another 20 h without stirring. The aged mixtures were filtered, washed, and dried at 100 °C overnight. After calcination at 500 °C for 5 h in air, the mesoporous products were obtained.

2.3. Characterization

In this work, additional characterization was performed in order to clearly establish the structural properties. Analytical techniques such as inductively coupled plasma-mass spectrometer, X-ray diffraction patterns, nitrogen physisorption isotherms, scanning electron microscopy, transmission electron microscopy, and zetasizer were used to characterize the synthesized mesoporous materials.

The elemental quantitative analysis was determined by inductively coupled plasma-mass spectrometer (ICP-MS, Agilent). In a typical analysis, 5 mg of samples (weighted by SCALTEC SBC with 0.1 mg accuracy) were dissolved in 10 ml acid mixture of HNO_3, $HClO_4$, and HF (5:3:2, v/v). The mixture was digested in a high-pressure bomb system at 170 °C for 5 h until a clear digested solution was obtained. After that, the resultant solution was transferred into a PTFE beaker and heated gently on a hot plate to evaporate the residual acid solvent. The residue was diluted by 2% HNO_3 (v/v) to 50 ml for ICP-MS analysis.

The crystalline structure of samples was characterized by X-ray diffraction (XRD) of Bruker Axs D8 Advance using Cu-Kα radiation (λ = 1.5406 Å, 40 kV, and 40 mA). Typically, the data were collected as low-angle patterns from 0.5° to 3° (2θ) with a step size of 0.002° and at a rate of 0.5 s/step, and wide-angle patterns from 20° to 80° (2θ) with a step size of 0.02° and at a rate of 0.5 s/step.

The surface area and porous structure were inferred from a surface analyzer of Quantachrome Nova 4200 Series. Samples were pretreated by degassing at 300 °C for 3 h prior to measurement. The

surface area was determined according to N_2 physisorption data at 77 K calculated by the BET (Brunauer–Emmett–Teller) method in the relative pressure range of 0.05–0.3. The pore size distribution was obtained using the BJH (Barrett–Joyner–Halenda) model assuming cylindrical geometry for the pores using a Harkins–Jura expression for the multilayer thickness. The total pore volume was taken from the volume of N_2 adsorbed at a relative pressure $P/P_0 = 0.995$ single point.

The morphologies of prepared samples were observed in scanning electron microscopy (SEM) of Hitachi S-4800. The pore and channel morphologies of the synthesized mesoporous materials were observed on a transmission electron microscopy (TEM, Philips TECNAI 20).

The zeta potentials of samples suspended in aqueous solution were measured using a Malvern Instruments' Zetasizer 2000 based on the method of electrophoretic light-scattering technique that measured migration rate of dispersed particles under the influence of an electric field. Suspensions of samples in DI water were prepared at variation pH. After five times of measurements, the average value and standard deviation of zeta potential were recorded.

2.4. Performance test

The batch equilibrium experiment was typically carried out to study the adsorption behavior by adding a fixed amount of SBA-15 or TiSBA-15 powders (50 mg) into 250 ml flasks containing 50 ml dye solution at different initial concentrations (0.05–0.5 mM). The flasks were agitated in an isothermal water-bath shaker at 150 rpm and 25 °C until equilibrium reached. Aqueous samples were collected by separation of powder from solution using PTFE filters. The dye concentration was determined on a double beam UV/vis spectrophotometer (PG Instruments UV-1880S) by measuring absorbance at specific wavelength for dyes. The amount of equilibrium adsorption, Q_e (mmol/g), was calculated by:

$$Q_e = \frac{(C_0 - C_e)V}{W} \quad (1)$$

where C_0 and C_e (mmol/L) were the liquid-phase concentrations of dye at initial and equilibrium conditions, respectively. V (L) was the volume of the dye solution and W (g) was the mass of dry sorbent used.

In a typical study of kinetic adsorption behavior, 50 mg of SBA-15 or TiSBA-15 were contacted with 50 ml of 0.5 mM dye solution using a water-bath shaker at 25 °C. The agitation speed was kept constant at 150 rpm. Solutions were analyzed to obtain the final concentration of dye at appropriate time intervals.

In order to prove that TiSBA-15 was a dual functional composite with adsorptive and catalytical capabilities, MB molecules as target compound were adsorbed onto the TiSBA-15 and then degraded by photocatalysis process to regenerate the TiSBA-15 powders. The experiments were conducted in a 100 ml cylindrical quartz reactor where 50 mg TiSBA-15 powders were suspended in a 50 ml of MB aqueous solution with an initial concentration of 0.025 mM. The mixture was first stirred for 60 min (the equilibrium adsorption time according to the adsorption kinetics as shown in SI Fig. S1) in dark at room temperature to assure the adsorption equilibrium reached, and the reaction solution was placed perpendicularly to a 400 W medium pressure mercury lamp (a wavelength range of 230–415 nm) under magnetic agitation. Solid samples were collected at particular time intervals, following filtration and the TOC concentration was determined by TOC analyzer (O.I. Analytical solids TOC Analyzer Model 1010).

A complete cycle was composed of adsorption and photocatalysis steps described above. The renewable TiSBA-15 powders after each cyclic run were collected and characterized by TOC, XRD, and N_2 sorption isotherm analyses. The cyclic efficiency is defined as the ratio of adsorption amount in each cyclic run to initial run.

3. Results and discussion

3.1. Characterization of prepared samples

The textural and structural properties of SBA-15 and TiSBA-15 are summarized in Table 1.

The powder low- and wide-angle XRD patterns of SBA-15 and TiSBA-15 samples prepared in different molar ratios of Si to Ti (nSi/nTi) are shown in Fig. 1a and b, respectively. Almost all samples exhibit typical low-angle diffraction patterns from mesoscopic *p6mm* symmetry formed by the 2D hexagonal array of mesoporous structure except for TiSBA-15[D]. These peaks assigned to (1 0 0), (1 1 0), and (2 0 0) at low-angle range are typical highly ordered SBA-15 with hexagonal *p6mm* structure which is in agreement with the reported pattern [25].

The d spacing at (1 0 0) planes and the length of the hexagonal unit cell a_0 are listed in Table 1 which are calculated using Bragg's law and the formula (1) as mentioned above. The observed $d_{(100)}$ spacing values from 12.76 to 12.51 nm for TiSBA-15[A]–[C] mean that the ordered mesostructure of SBA-15 is still maintained after a limited content of titanium atoms introduced into the framework. The poorly resolved XRD pattern and disappeared intense peaks of TiSBA-15[D] indicate the decrease in the structural integrity.

As shown in Fig. 1b, no peaks attributed to crystalline silica in the wide-angle XRD patterns indicate a mesoporous structure with amorphous silica walls. The appearance of specific peaks at $2\theta = 25.3°$, 37.8°, 48.3°, 54.8°, and 63.4° are ascribed to the anatase

Table 1
Physical and chemical properties of SBA-15 and TiSBA-15.

Sample	Chemical composition			Textural properties			Structural properties		
	Si/Ti[a] (at%)	Si/Ti[b] (at%)	Ti[c] (wt%)	S_{BET}[d] (m^2/g, $n=3$)	D_p[e] (nm, $n=3$)	V_p[f] (cm^3/g, $n=3$)	$d_{(100)}$[g] (nm)	a_0[h] (nm)	Wt[i] (nm)
SBA-15	–	–	–	659 ± 45	5.27 ± 0.19	0.83 ± 0.05	9.73	11.23	5.96
TiSBA-15[A]	7	74.6	1.26	918 ± 85	6.11 ± 0.22	1.09 ± 0.11	11.05	12.76	6.65
TiSBA-15[B]	5	41.6	2.24	958 ± 19	6.28 ± 0.02	1.08 ± 0.03	10.93	12.62	6.34
TiSBA-15[C]	3	6.33	12.3	663 ± 30	6.31 ± 0.02	0.82 ± 0.05	10.83	12.51	6.2
TiSBA-15[D]	1	2.11	27.0	455 ± 5.5	3.82 ± 0.02	0.57 ± 0.05	–	–	–

[a] Molar ratio of nSi/nTi in synthesis gel.
[b] Molar ratio of nSi/nTi in final product.
[c] Weight percentage of titanium in final product determined by ICP-MS analysis.
[d] Specific surface area calculated by the BET method.
[e] Mean pore size calculated by the BJH method.
[f] Total pore volume recorded at $P/P_0 = 0.995$.
[g] The d spacing measured by XRD and calculated by Bragg's law: $\lambda = 2d_{(100)} \sin\theta$.
[h] Unit cell parameter calculated as the formula (1): $a_0 = 2d_{(100)}/\sqrt{3}$.
[i] Pore wall thickness calculated as $Wt = a_0 - D_p$.

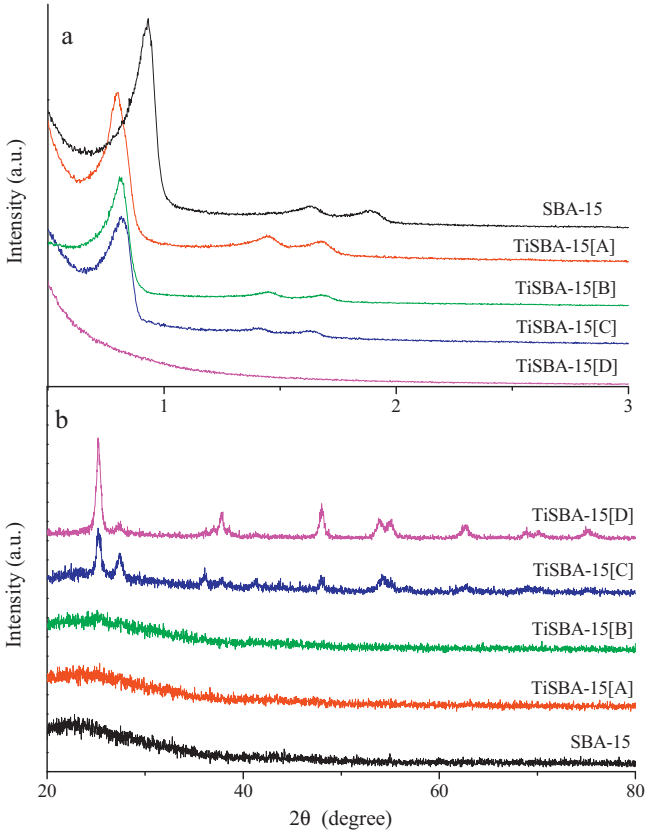

Fig. 1. (a) Low-angle and (b) wide-angle XRD patterns of SBA-15 and TiSBA-15.

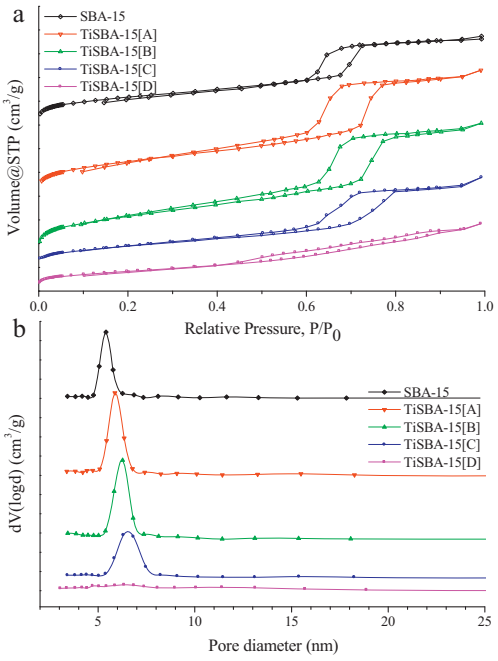

Fig. 2. (a) N_2 sorption isotherms and (b) pore diameter distribution of SBA-15 and TiSBA-15.

phase of TiO_2 [28] when the molar ratios of Si/Ti are above 3. The XRD results imply that limited amount of titanium can be successfully incorporated into the silicate framework of SBA-15 under the experimental condition in this study. The increasing titanium content in the synthesis gels tends to form extraframework TiO_2 of anatase phase and results in the disappearance in low-angle Bragg's peaks.

Fig. 2a shows the nitrogen adsorption–desorption isotherms of SBA-15 and TiSBA-15 with different titanium loadings. Regarding the textural properties, all samples except TiSBA-15[D] displayed similar inflection points and a hysteresis loop. It is well studied that the location of inflection point is related to the pore scale. The hysteresis loops of Type H1 are evidence of mesoporosity-indeed and characteristic features of the Type IV isotherm. A step change at higher relative pressures of 0.6–0.75 is due to desorption of nitrogen and capillary condensation in the pore structure. The sharpness of steps also displays the uniformity of the mesopore size distribution. This indicates a typical mesoporous material with larger pore sizes and narrow size distributions [29]. However, some differences between the prepared samples are observed. The surface areas of TiSBA-15[A] and TiSBA-15[B] are higher than the original SBA-15 which may be attributed to the larger pore diameter and pore volume of the titanium-containing samples. The observed increase in the surface area upon Ti substitution is in accordance with the reported work [30]. The TiSBA-15[A] and TiSBA-15[B] exhibit similar values of specific surface area due to a similar feature of adsorption isotherms. The isotherm intensity of TiSBA-15[C] is lower than that of TiSBA-15[A] and TiSBA-15[B] because the accumulation of TiO_2 particles on the surface of samples decreases specific surface area and pore volume of TiSBA-15[C]. TiSBA-15[D] presents a Type II isotherm which is a characteristic of non-porous or macroporous. It may be concluded that a lot of TiO_2 particles blockade and destroy the uniform structure to worm-like structure during the synthesis process.

Fig. 2b depicts the pore size distributions of SBA-15 and TiSBA-15 by the BJH analysis of adsorption branches. A narrow pore size distribution in mesopore range observed from SBA-15, TiSBA-15[A]–[C] samples indicates the presence of mesoporous channels, while a wide range distribution observed from TiSBA-15[D] displays no mesostructure. Therefore, the decrease of *n*Si/*n*Ti molar ratio tends to shift the pore diameter distribution to a wide region as observed in Fig. 2b. It is also found that the pore size of TiSBA-15[A] and TiSBA-15[B] is greater than the original SBA-15. For TiSBA-15[C], the mesostructure is maintained and the pore diameter is increased even though the titania particles somewhat blockade its mesopores, which is also corresponding to the above XRD results.

Fig. 3 presents the SEM images of SBA-15 and TiSBA-15 materials with different Si/Ti ratios. The particles of prepared SBA-15 are joined to form long fibrous macrostructures with a relatively particle size of several micrometers, the typical morphology of SBA-15 [25]. Almost no change in morphology and structure is observed for TiSBA-15[A] and TiSBA-15[B] compared to SBA-15. When Si/Ti ratio is decreased to 3 (TiSBA-15[C]), the twine-like macroporous structure is less resolved with visible particles on the external surface by SEM observation (Fig. 3d). These aggregated particles with relatively smaller size are suggested to be anatase titania evidenced by the result of wide-angle XRD pattern. If the Si/Ti ratio is further decreased to 1 (TiSBA-15[D]), no more fibers can be directly observed by SEM images (Fig. 3e). As a result, the addition of titanium has a strong influence on the formation of mesoporous structure, and a limited content of titanium can be incorporated into the SBA-15 framework successfully without structural changes.

The highly ordered mesostructure can be further confirmed by TEM analysis. The TEM images from SBA-15 (Fig. 4a) clearly shows well-ordered pores and cylindrical channels taken along the (1 1 0) and (1 0 0) directions, indicative of 2D hexagonal *p6mm* mesostructure. In addition, TiSBA-15[A] and TiSBA-15[B] samples also display the same arrays as SBA-15 (as shown in Fig. 4b and c). The estimated pore diameter of about 5–6 nm, center-to-center

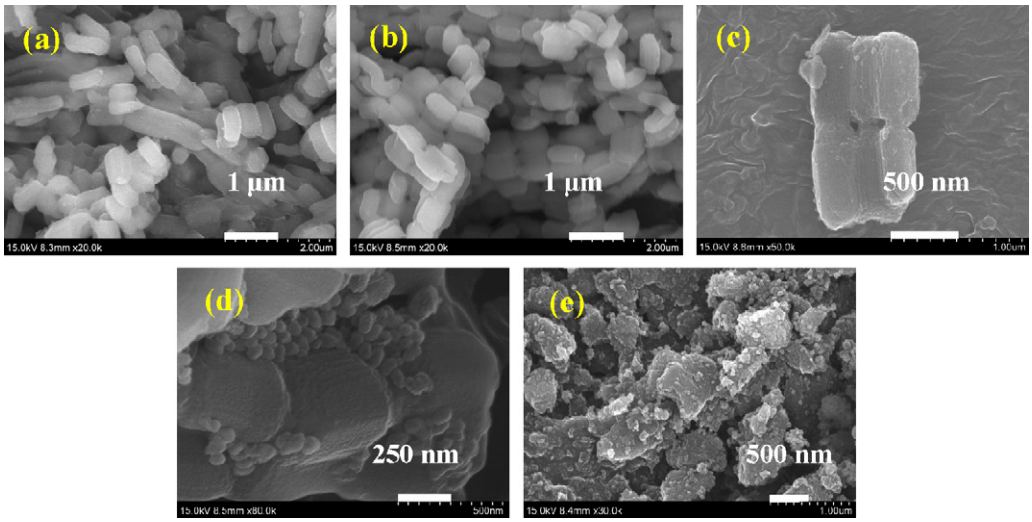

Fig. 3. SEM images of (a) SBA-15, (b) TiSBA-15[A], (c) TiSBA-15[B], (d) TiSBA-15[C], and (e) TiSBA-15[D].

pore distance (a_0) of 11–12 nm, and pore wall thickness of 6–7 nm are observed. These results are in accordance with those measured from N_2 sorption analysis and the low-angle XRD patterns. For TiSBA-15[C], the periodic structure of the silicate framework is kept unaffected (as shown in Fig. 4d). The textural and structural properties such as pore diameter, distance between two consecutive centers of hexagonal pores, and pore wall thickness also confirm the above-mentioned BJH and XRD results. Besides, some dark spots corresponding to TiO_2 particles are presented inside the stripe patterns of TiSBA-15[C] structure, indicating the aggregation of excess titanium ions. The morphology also interprets why TiSBA-15[C] simultaneously presents signals of representative hexagonal structure and anatase TiO_2 observed in XRD patterns. The growth of TiO_2 particles may blockade the mesopore and decrease the specific surface area. Moreover, the morphology of TiSBA-15[D] in Fig. 4e displays a distortion of framework which results in the chaotic structure. The disordered wormhole-like arrangement also consists with the result of SEM image in Fig. 3e.

3.2. Adsorption behavior on SBA-15 and TiSBA-15

The equilibrium adsorption isotherm is the basic requirement in the design of adsorption systems [31]. In this study, the Langmuir and the Freundlich are applied to represent the sorption behavior on SBA-15 and TiSBA-15. The Langmuir isotherm model [32] is based on assumptions that monolayer coverage of adsorbate occurs over homogeneous sites and a saturation point is reached where no further adsorption can act. The Freundlich isotherm model [33] is an empirical equation employed to describe heterogeneous system. Both isotherm models and linearized forms are represented as following equations. The Langmuir constants Q_{max} and K_L can be calculated by the plot of $1/Q_e$ versus $1/C_e$ with slope $1/Q_{max}$ and intercept $1/(Q_{max}K_L)$, while the Freundlich constants K_F and n_F are obtained by plotting $\log Q_e$ versus $\log C_e$.

(1) Langmuir model:

$$Q_e = \frac{Q_{max}K_L C_e}{1 + K_L C_e} \tag{2}$$

Linearized form:

$$\frac{1}{Q_e} = \left(\frac{1}{Q_{max}K_L}\right)\left(\frac{1}{C_e}\right) + \frac{1}{Q_{max}} \tag{3}$$

(2) Freundlich model:

$$Q_e = K_F C_e^{1/n_F} \tag{4}$$

Linearized form:

$$\log Q_e = \frac{1}{n_F}\log C_e + \log K_F \tag{5}$$

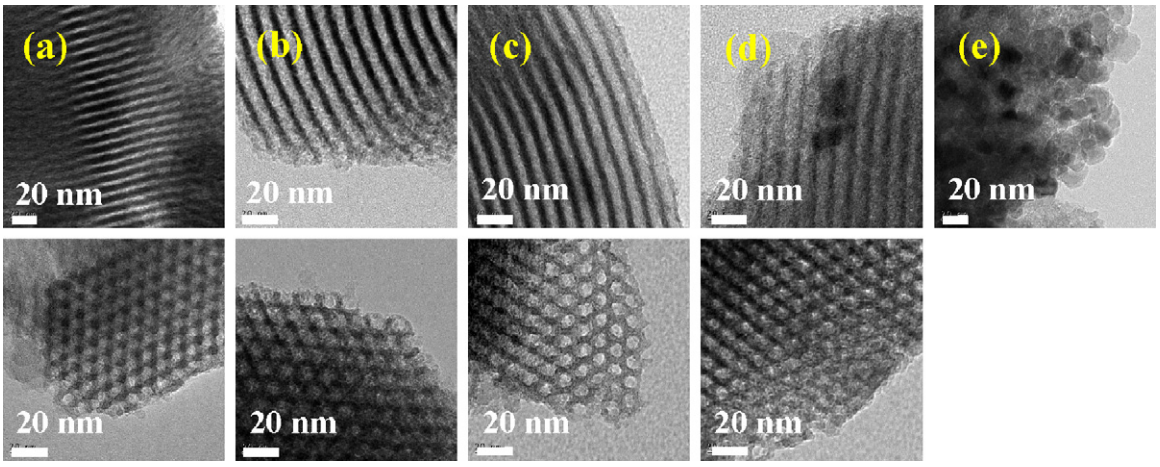

Fig. 4. TEM images of (a) SBA-15, (b) TiSBA-15[A], (c) TiSBA-15[B], (d) TiSBA-15[C], and (e) TiSBA-15[D].

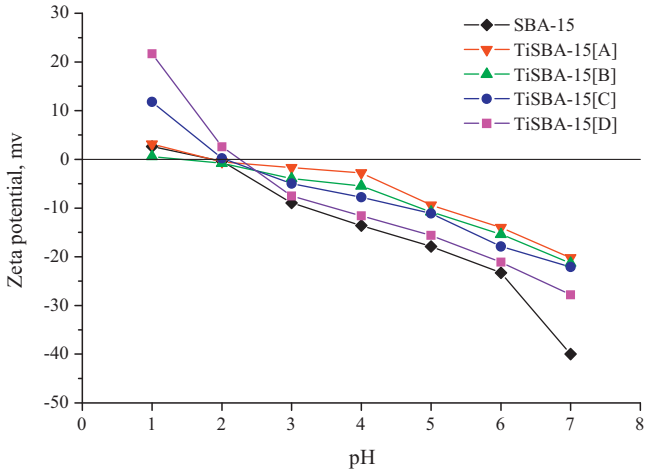

Fig. 5. Zeta potentials of SBA-15 and TiSBA-15 at various pH values.

where Q_e is the adsorption capacity of the adsorbent (mmol/g); C_e is the equilibrium concentration of adsorbate in solution (mmol/L); Q_{max} is the maximum monolayer adsorption capacity (mmol/g); K_L is the adsorption equilibrium constant related to the affinity of the binding sites and energy of adsorption (L/mmol); K_F ((mmol/g) × (g/m^{-3})$^{-1/n_F}$) and n_F are Freundlich constant and index number for a given adsorbate and adsorbent at specific temperature, indicative of the extent of adsorption and the degree of nonlinearity between solution concentration and adsorption, respectively.

An equilibrium parameter or dimensionless constant separation factor R_L is also applied to reveal the type of isotherm which is defined as follows [34]:

$$R_L = \frac{1}{1 + K_L C_0} \quad (6)$$

where C_0 is the highest initial dye concentration (mmol/L). The adsorption behavior is (1) unfavorable as $R_L > 1$; (2) linear as $R_L = 1$; (3) favorable as $1 > R_L > 0$; (4) irreversible as $R_L = 0$. The value of n_F in the range of 1–10 also indicates favorable adsorption [35].

Fig. 5 displays the zeta potentials of SBA-15 and TiSBA-15 in various pH values. All materials are negative surface charged when pH value above 3 and the negative charge density decreases with the increasing pH. Meanwhile, MB exhibits an aqueous pH range of 5.51–5.75 which favors the adsorption by electrostatic attraction [36]. Therefore, MB as a cationic dye was chosen and used to thoroughly investigate the sorption capacity of prepared materials. The equilibrium data of MB on SBA-15 and TiSBA-15 samples in aqueous pH at 25 °C and the fitted curves by Langmuir and Freundlich models are depicted in Fig. 6. The Langmuir and Freundlich constants and the linear regression correlations (r^2) for both isotherm models are listed in Table 2. As shown in Fig. 6, the adsorption isotherms of MB on different materials are quite close and can be fitted very well by both isotherm models. The linear regression correlation coefficient, $r^2 > 0.9$, suggests a good fit in the isotherms by the model used. The calculated Langmuir isotherm constant Q_{max} of each material is in agreement with its experimental result (Q_e). The values of R_L (dimensionless constant separation factor) are evaluated in the range of 0.05–0.15 indicating a favorable adsorption process of MB on SBA-15 and various TiSBA-15.

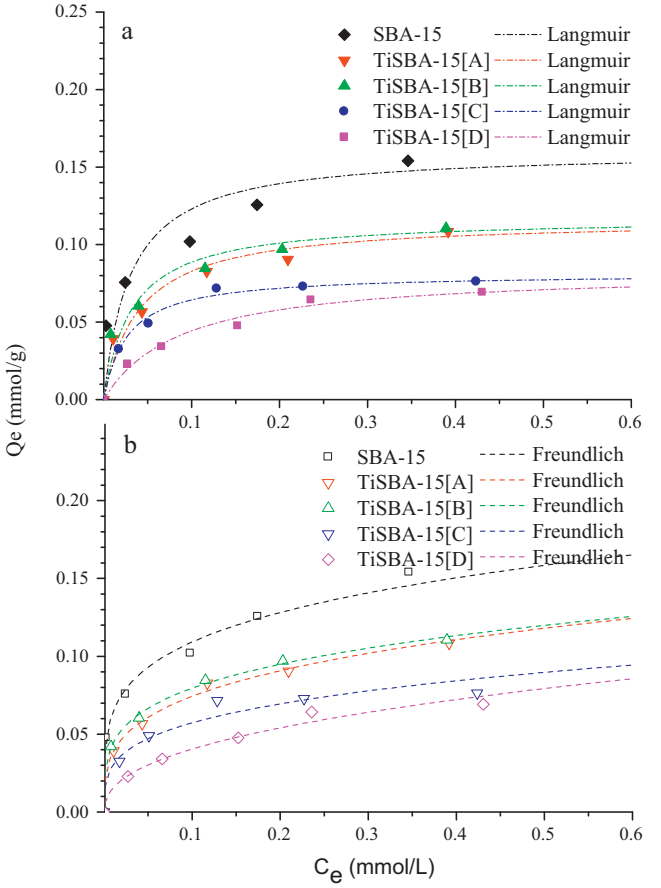

Fig. 6. Adsorption isotherms of MB on SBA-15 and TiSBA-15 fitted by (a) Langmuir model and (b) Freundlich model.

It is observed that the adsorption capacity of TiSBA-15[A] is similar to that of TiSBA-15[B] (0.108 and 0.110 mmol/g, respectively) and reduces significantly to the values of 0.076 of TiSBA-15[C] and 0.069 mmol/g of TiSBA-15[D]. It can probably be ascribed to the reduction of specific surface as well as the adsorptive site on the composites. A higher adsorption capacity of SBA-15 (0.154 mmol/g) than that of TiSBA-15 is also observed. It can be explained by the effect of electrostatic attraction and adsorption intensity. As shown in Fig. 5, the zeta potential of SBA-15 is more negative than that of TiSBA-15 materials within a pH range of 5.51–5.75 for nature MB solution, that is to say, a higher surface charge density is revealed on SBA-15. Therefore, the strong dependence of adsorption on these mesoporous materials suggests that the

Table 2
Langmuir and Freundlich parameters for adsorption on SBA-15 and TiSBA-15.

MB	Q_e (mmol/g)	Langmuir isotherm				Freundlich isotherm		
		Q_{max} (mmol/g)	K_L (L/mmol)	R_L	r^2	K_F ((mmol/g) × (g/m^{-3})$^{-1/n_F}$)	n_F	r^2
SBA-15	0.154	0.160	33.03	0.06	0.976	0.185	4.33	0.987
TiSBA-15[A]	0.108	0.116	24.85	0.07	0.989	0.144	3.90	0.992
TiSBA-15[B]	0.110	0.117	31.00	0.06	0.992	0.143	3.92	0.995
TiSBA-15[C]	0.076	0.081	37.70	0.05	0.998	0.108	3.58	0.917
TiSBA-15[D]	0.069	0.080	11.36	0.15	0.987	0.106	2.38	0.980

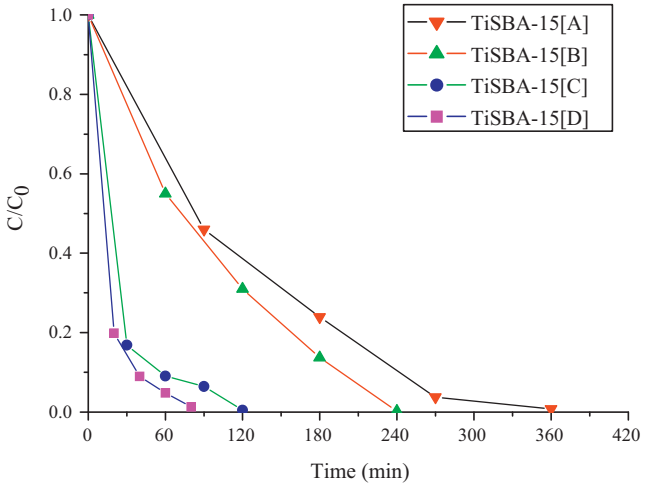

Fig. 7. TOC variations with mineralization of MB on TiSBA-15.

sorption capacity is a function of the electrostatic attraction. It is noteworthy that the Freundlich constant n_F corresponds to the adsorption intensity. As listed in Table 2, all the values of calculated n_F are greater than 1, which indicates the cationic molecules favorably adsorbed on all materials. This is in great accordance with the findings from separation factor R_L. Besides, n_F is also observed to follow the sequence of SBA-15 > TiSBA-15[A] ≒ TiSBA-15[B] > TiSBA-15[C] > TiSBA-15[D], which may explain why adsorption capacity of SBA-15 is much larger than that of other TiSBA-15 samples in this study.

3.3. Dye removal by TiSBA-15

Photocatalytic degradation was performed in aqueous solutions in the presence of MB adsorbed on TiSBA-15 under UV light radiation. The TOC on TiSBA-15 was determined to evaluate the adsorption as well as photocatalytic behavior on the surface of composites. MB photodegradation at an initial concentration of 0.025 mmol/g was performed for the analysis. On the previous adsorption experiment, 0.025 mM MB was found to be completely adsorbed on TiSBA-15. The degradation curves of TOC on TiSBA-15 materials are depicted in Fig. 7. The Langmuir–Hinshelwood kinetic model [37] is generally utilized in the photo-oxidation process and the degradation rate is described by the following equation:

$$r = -\frac{dC}{dt} = \frac{k_r K_{ads} C}{1 + K_{ads} C} = kC \quad (7)$$

$$\ln\left(\frac{C}{C_0}\right) = -kt \quad (8)$$

where C is the concentration of the reactant (mmol/L), t is the UV illumination time, k_r is the reaction rate constant (mmol L^{-1} min^{-1}), K_{ads} is the adsorption coefficient of the reactant (L/mmol), and k is the observed reaction rate constant (min^{-1}). Eq. (7) can be integrated at the boundary of initial state and a given time t, resulting in a form as Eq. (8). The slope of plotting $\ln(C/C_0)$ versus t gives to the degradation rate. Accordingly, the degradation rate of MB adsorbed on TiSBA-15 is determined and listed in Table 3. For a given amount of dyes, a larger rate constant k indicates that less time is demanded for a total mineralization and a complete regeneration of the TiSBA-15.

Table 3
Degradation rate of MB adsorbed on TiSBA-15.

	k_1 (min^{-1})	k_2 (min^{-1} gTi^{-1})	r^2
TiSBA-15[A]	0.0080	12.69	0.9975
TiSBA-15[B]	0.0145	12.94	0.9998
TiSBA-15[C]	0.0400	6.50	0.9285
TiSBA-15[D]	0.0604	4.47	0.9630

Table 4
Regeneration efficiency (%) by re-adsorption of MB on TiSBA-15.

Run no.	TiSBA-15[A]	TiSBA-15[B]	TiSBA-15[C]	TiSBA-15[D]
1	100	100	100	100
2	99.3	98.8	98.7	98.9
3	98.8	98.5	98.2	98.8
4	98.5	98.2	98.1	98.4

As shown in Fig. 7, all of the samples show photocatalytic activity. As listed in Table 3, the kinetic rate (k_1) depends on the Ti content in the TiSBA-15 materials. It should be noted that more anatase TiO_2 particles are formed and located on the external surface of TiSBA-15[D], more accessible to the target substrate. Therefore, the better performance in the removal rate should be attributed to the formation of TiO_2 particles on the external surface. If we normalize the photodegradation rate by per gram of Ti contained in synthesized catalysts, the kinetic rate (k_2) follows the order of TiSBA-15[A] ≒ TiSBA-15[B] > TiSBA-15[C] > TiSBA-15[D]. This exceptional activity is attributed to higher adsorption ability resulted from larger specific surface area and better ordered mesostructure of TiSBA-15[A] and [B].

It is clearly seen that the initial blue powders are gradually decolored to the white powders during the photocatalytical experiment (as shown in SI Fig. S2). Therefore, TiSBA-15 materials can be regenerated by photocatalysis process according to the TOC variation and decolorization phenomenon.

A cyclic recovery test of MB adsorbed on the renewable TiSBA-15 after photocatalytically regeneration is evaluated. The regeneration efficiency is calculated and listed in Table 4. After cyclic runs, all materials still maintain an efficiency of nearly 100%, which indicates that a thorough regeneration of TiSBA-15 can be achieved easily.

Samples after four cyclic runs were characterized by XRD analysis and N_2 adsorption–desorption isotherms. Fig. 8 shows the low-angle XRD patterns of four different TiSBA-15 samples before and after cyclic runs. The characteristic peaks still remain in the patterns of all regenerated materials except for TiSBA-15[D]. The textural properties of the samples are also listed in Table 5. A slight decrease in properties is observed for all used samples. This may demonstrate that the TiSBA-15 has a durable structure during the adsorption and regeneration process.

Table 5
Physical and chemical properties of TiSBA-15 before and after cyclic runs.

Sample	Surface area (m^2/g, n = 3)		Pore diameter (nm, n = 3)		Pore volume (cm^3/g, n = 3)	
	Before	After	Before	After	Before	After
TiSBA-15[A]	918 ± 85	858 ± 62	6.11 ± 0.22	6.03 ± 0.02	1.09 ± 0.11	0.96 ± 0.08
TiSBA-15[B]	958 ± 19	863 ± 55	6.28 ± 0.02	6.14 ± 0.06	1.08 ± 0.03	0.95 ± 0.03
TiSBA-15[C]	663 ± 30	660 ± 19	6.31 ± 0.02	6.20 ± 0.05	0.82 ± 0.05	0.77 ± 0.03
TiSBA-15[D]	455 ± 5.5	433 ± 63	3.82 ± 0.02	3.20 ± 0.02	0.57 ± 0.05	0.40 ± 0.05

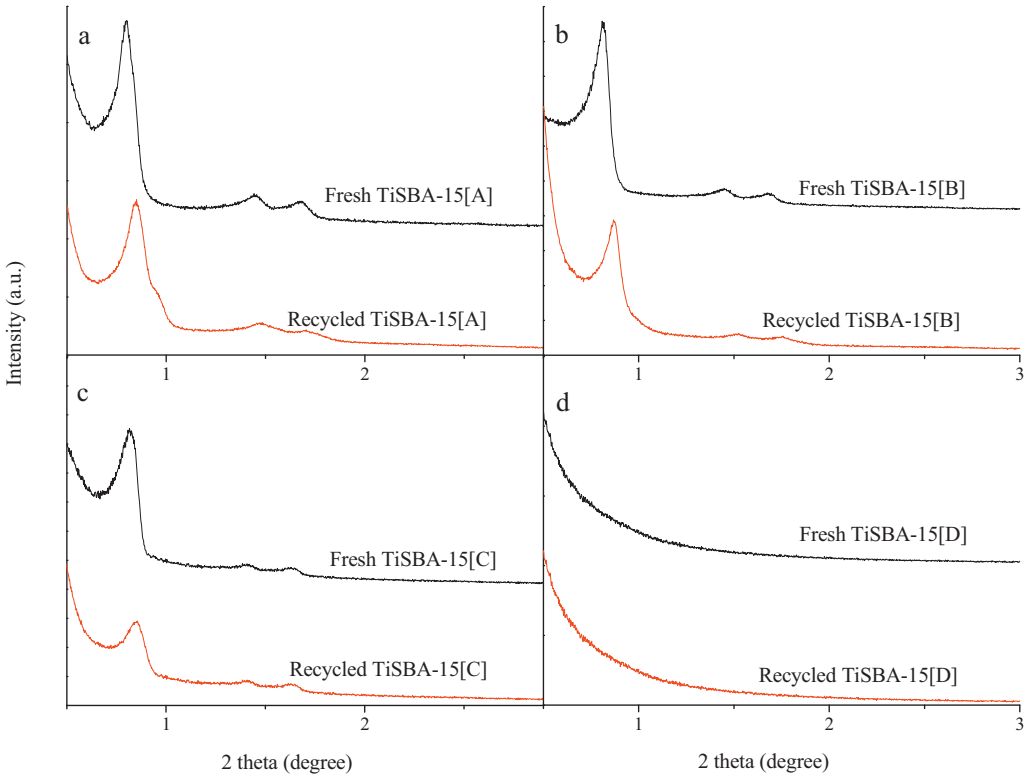

Fig. 8. Low-angle XRD patterns of fresh and recycled TiSBA-15.

It is concluded that TiSBA-15 exhibits advantages of adsorptive ability from mesoporous structure and photocatalytic performance by Ti-incorporated into the framework. The organic molecules are largely adsorbed onto TiSBA-15 materials and then photo-degraded under UV irradiation. The process can be effectively recycled due to the regeneration capability of TiSBA-15. As a result, TiSBA-15 can be considered an ideal and effective material to remove organic pollutants in aqueous solution due to the synergetic effect of both adsorption and catalysis. It means that organic pollutants can be adsorbed or concentrated in situ and then degraded in vitro under factory process, while the mesoporous composites are regenerated and recycled.

4. Conclusions

In this study, the results show that a limited content of Ti ions can successfully be incorporated into the framework of SBA-15 without provoking the mesoporous structure. Anatase TiO_2 has been formed and located on the external surface of SBA-15 with *n*Si/*n*Ti value below 3. The analysis of adsorption behavior shows that the SBA-15 and TiSBA-15 are effective adsorbents for MB removal from aqueous solutions due to their high adsorption capacity. The adsorption isotherms can be well fitted with Langmuir and Freundlich models. The sorption capacity of MB follows the order of SBA-15 > TiSBA-15[A] ≒ TiSBA-15[B] > TiSBA-15 [C] > TiSBA-15[D]. The higher adsorption capacity of SBA-15 than that of TiSBA-15 is due to the effect of electrostatic attraction which is benefit to the adsorption intensity. The photodegradation of MB depends on the Ti content in the TiSBA-15 materials. However, TiSBA-15[A] and [B] exhibit better photodegradation rate normalized by per gram of Ti in synthesized samples. This photocatalytic behavior could be attributed to synergistic effect with adsorptive ability. After photocatalytic illumination, the structural regularity of TiSBA-15 is still maintained.

TiSBA-15 exhibits advantages of adsorptive ability from mesoporous structure and photocatalytic performance by Ti-incorporated into the framework. The organic molecules are largely adsorbed onto TiSBA-15 materials and then photo-degraded under UV irradiation. The process can be effectively recycled due to the regeneration capability of TiSBA-15. As a result, TiSBA-15 can be considered an ideal and effective material to remove organic pollutants in aqueous solution due to the synergetic effect of both adsorption and catalysis. Organic pollutants are supposed to be adsorbed or concentrated in situ and then degraded in vitro under factory process, while the mesoporous composites are regenerated and recycled.

Acknowledgement

The authors would like to appreciate and express deep gratitude to the Institute of Nuclear Energy Research for the support of techniques of characterization in this work.

Appendix A. Supplementary data

Supplementary data associated with this article can be found, in the online version, at doi:10.1016/j.jhazmat.2010.11.125.

References

[1] E. Lorenc-Grabowska, G. Gryglewicz, Adsorption characteristics of Congo Red on coal-based mesoporous activated carbon, Dyes Pigm. 74 (2007) 34–40.
[2] V.K. Gupta, Suhas, Application of low-cost adsorbents for dye removal – a review, J. Environ. Manage. 90 (2009) 2313–2342.
[3] A.A. Attia, B.S. Girgis, S.A. Khedr, Capacity of activated carbon derived from pistachio shells by H_3PO_4 in the removal of dyes and phenolics, J. Chem. Technol. Biotechnol. 78 (2003) 611–619.
[4] I.A.W. Tan, A.L. Ahmad, B.H. Hameed, Adsorption of basic dye using activated carbon prepared from oil palm shell: batch and fixed bed studies, Desalination 225 (2008) 13–28.

[5] A. Rodríguez, J. García, G. Ovejero, M. Mestanza, Adsorption of anionic and cationic dyes on activated carbon from aqueous solutions: equilibrium and kinetics, J. Hazard. Mater. 172 (2009) 1311–1320.
[6] B. Armağan, O. Özdemir, M. Turan, M.S. Celik, The removal of reactive azo dyes by natural and modified zeolites, J. Chem. Technol. Biotechnol. 78 (2003) 725–732.
[7] A.B. Engin, Ö. Özdemir, M. Turan, A.Z. Turan, Color removal from textile dyebath effluents in a zeolite fixed bed reactor: determination of optimum process conditions using Taguchi method, J. Hazard. Mater. 159 (2008) 348–353.
[8] S.A. Avlonitis, I. Poulios, D. Sotiriou, M. Pappas, K. Moutesidis, Simulated cotton dye effluents treatment and reuse by nanofiltration, Desalination 221 (2008) 259–267.
[9] J. Sun, Y. Hu, Z. Bi, Y. Cao, Simultaneous decolorization of azo dye and bioelectricity generation using a microfiltration membrane air-cathode single-chamber microbial fuel cell, Bioresour. Technol. 100 (2009) 3185–3192.
[10] L. Zheng, Y. Su, L. Wang, Z. Jiang, Adsorption and recovery of methylene blue from aqueous solution through ultrafiltration technique, Sep. Purif. Technol. 68 (2009) 244–249.
[11] W. Lau, A.F. Ismail, Polymeric nanofiltration membranes for textile dye wastewater treatment: preparation, performance evaluation, transport modeling, and fouling control – a review, Desalination 245 (2009) 321–348.
[12] J. Wu, C. Liu, K.H. Chu, S. Suen, Removal of cationic dye methyl violet 2B from water by cation exchange membranes, J. Membr. Sci. 309 (2008) 239–245.
[13] Y. Zhou, Z. Liang, Y. Wang, Decolorization and COD removal of secondary yeast wastewater effluents by coagulation using aluminum sulfate, Desalination 225 (2008) 301–311.
[14] Q.Y. Yue, B.Y. Gao, Y. Wang, H. Zhang, X. Sun, S.G. Wang, R.R. Gu, Synthesis of polyamine flocculants and their potential use in treating dye wastewater, J. Hazard. Mater. 152 (2008) 221–227.
[15] C.A. Martínez-Huitle, E. Brillas, Decontamination of wastewaters containing synthetic organic dyes by electrochemical methods: a general review, Appl. Catal. B: Environ. 87 (2009) 105–145.
[16] J. Sun, S. Shi, Yi. Lee, S. Sun, Fenton oxidative decolorization of the azo dye Direct Blue 15 in aqueous solution, Chem. Eng. J. 155 (2009) 680–683.
[17] E.R. Bandala, L. Brito, M. Pelaez, Degradation of domic acid toxin by UV-promoted Fenton-like processes in seawater, Desalination 245 (2009) 135–145.
[18] U.G. Akpan, B.H. Hameed, Parameters affecting the photocatalytic degradation of dyes using TiO_2-based photocatalysts: a review, J. Hazard. Mater. 170 (2009) 520–529.
[19] P. Gayathri, R.P.J.D. Dorathi, K. Palanivelu, Sonochemical degradation of textile dyes in aqueous solution using sulphate radicals activated by immobilized cobalt ions, Ultrason. Sonochem. 17 (2010) 566–571.
[20] A.H. Konsowa, M.E. Ossman, Y. Chen, J.C. Crittenden, Decolorization of industrial wastewater by ozonation followed by adsorption on activation carbon, J. Hazard. Mater. 176 (2010) 181–185.
[21] R. Ahmad, P.K. Mondal, S.Q. Usmani, Hybrid UASFB-aerobic bioreactor for biodegradation of acid yellow-36 in wastewater, Bioresour. Technol. 101 (2010) 3787–3790.
[22] L. Pereira, A.V. Coelho, C.A. Viegas, M.M. Correia dos Santos, M.P. Robalo, L.O. Martins, Enzymatic biotransformation of the azo dye Sudan Orange G with bacterial CotA-laccase, J. Biotechnol. 139 (2009) 68–77.
[23] M.A. Zanjanchi, H. Golmojdeh, M. Arvand, Enhanced adsorptive and photocatalytic achievements in removal of methylene blue by incorporating tungstophosphoric acid–TiO_2 into MCM-41, J. Hazard. Mater. 169 (2009) 233–239.
[24] V. Belessi, G. Romanos, N. Boukos, D. Lambropoulou, C. Trapalis, Removal of Reactive Red 195 from aqueous solutions by adsorption on the surface of TiO_2 nanoparticles, J. Hazard. Mater. 170 (2009) 836–844.
[25] D.Y. Zhao, J.L. Feng, Q.S. Huo, N. Melosh, G.H. Fredrickson, B.F. Chmelka, G.D. Stucky, Triblock copolymer syntheses of mesoporous silica with periodic 50 to 300 Angstrom pores, Science 279 (1998) 548–552.
[26] W. Dong, C.W. Lee, X. Lu, Y. Sun, W. Hua, G. Zhuang, S. Zhang, J. Chen, H. Hou, D. Zhao, Synchronous role of coupled adsorption and photocatalytic oxidation on ordered mesoporous anatase TiO_2–SiO_2 nanocomposites generating excellent degradation activity of RhB dye, Appl. Catal. B: Environ. 95 (2010) 197–207.
[27] A. Vinu, P. Srinivasu, M. Miyahara, K. Ariga, Preparation and catalytic performances of ultralarge-pore TiSBA-15 mesoporous molecular sieves with very high Ti content, J. Phys. Chem. B 110 (2006) 801–806.
[28] L.Q. Jing, X.J. Sun, W.M. Cai, Z.L. Xu, Y.G. Du, H.G. Fu, The preparation and characterization of nanoparticle TiO_2/Ti films and their photocatalytic activity, J. Phys. Chem. Solids 64 (2003) 615–623.
[29] K.S.W. Sing, D.H. Everett, R.A.W. Haul, L. Moscou, R.A. Pierotti, J. Rouquérol, T. Siemieniewska, Reporting physisorption data for gas/solid systems with special reference to the determination of surface area and porosity, Pure Appl. Chem. 57 (1985) 603–619.
[30] G. Li, X.S. Zhao, Characterization and photocatalytic properties of titanium-containing mesoporous SBA-15, Ind. Eng. Chem. Res. 45 (2006) 3569–3573.
[31] M.H. Stenzel, Remove organics by activated carbon adsorption, Chem. Eng. Prog. 89 (1993) 36–43.
[32] I. Langmuir, The constitution and fundamental properties of solids and liquids. II. Liquids, J. Am. Chem. Soc. 39 (1917) 1848–1906.
[33] H.M.F. Freundlich, Over the adsorption in solution, J. Phys. Chem. 57 (1906) 385–470.
[34] G. McKay, Adsorption of dyestuffs from aqueous solutions with activated carbon I: equilibrium and batch contact-time studies, J. Chem. Technol. Biotechnol. 32 (1982) 759–772.
[35] V. Vadivelan, K.V. Kumar, Equilibrium, kinetics, mechanism, and process design for the sorption of methylene blue onto rice husk, J. Colloid Interface Sci. 286 (2005) 90–100.
[36] C.H. Huang, K.P. Chang, H.D. Ou, Y.C. Chiang, C.F. Wang, Adsorption of cationic dyes onto mesoporous silica, Microporous Mesoporous Mater., in press, doi:10.1016/j.micromeso.2010.11.002.
[37] M. Trillas, J. Peral, X. Domènech, Redox photodegradation of 2,4-dichlorophenoxyacetic acid over TiO_2, Appl. Catal. B: Environ. 5 (1995) 377–387.